JOURNAL OF SYNCHROTRON RADIATION

ISSN 1600-5775

Received 21 December 2018
Accepted 19 June 2019

Edited by M. Zangrando, IOM-CNR and Elettra-Sincrotrone, Italy

[1] This article will form part of a virtual special issue containing papers presented at the PhotonDiag2018 workshop.

Keywords: X-ray imaging; beam diagnostics; X-ray free-electron lasers; beam transport systems; scintillators.

Operation of photon diagnostic imagers for beam commissioning at the European XFEL[1]

Andreas Koch,* Johannes Risch, Wolfgang Freund, Theophilos Maltezopoulos, Marc Planas and Jan Grünert

European XFEL, 22869 Schenefeld, Germany. *Correspondence e-mail: andreas.koch@xfel.eu

X-ray photon beam diagnostic imagers are located at 24 positions in the European XFEL beam transport system to characterize the X-ray beam properties, and to give feedback for tuning and optimization of the electron acceleration and orbit, the undulators, and the X-ray optics. One year of commissioning allowed experience to be gained with these imagers, which will be reported here. The sensitive Spontaneous Radiation imager is useful for various investigations in spontaneous radiation mode: for undulator adjustments and for low-signal imaging applications. The high-resolution Free-Electron Laser imager, 10 µm spatial resolution, is extensively used for the monitoring of beam position, spot size and shape, gain curve measurements, and also for beam-intensity monitoring. The wide field-of-view pop-in monitors (up to 200 mm) are regularly used for alignment and tuning of the various X-ray optical components like mirrors, slits and monochromators, and also for on-line beam control of a stable beam position at the instruments. The Exit Slit imager after the soft X-ray monochromator provides spectral information of the beam together with multi-channel plate based single-pulse gating. For particular use cases, these special features of the imagers are described. Some radiation-induced degradation of scintillators took place in this initial commissioning phase, providing useful information for better understanding of damage thresholds. Visible-light radiation in the beam pipe generated by upstream bending magnets caused spurious reflections in the optical system of some of the imagers which can be suppressed by aluminium-coated scintillating screens.

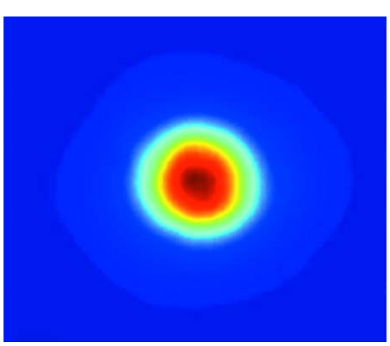

1. Introduction

Photon-beam diagnostics at the European XFEL are installed for monitoring the free-electron laser (FEL) beam along the beam path at specific locations related to the X-ray optical elements. This means that 24 photon diagnostic imagers are operating to visualize the beam and provide information on position, shape, stability, intensity and spectral properties of the beam. The X-ray beam is delivered to six scientific instruments (Tschentscher *et al.*, 2017; Grünert *et al.*, 2019).

The photon diagnostic imagers (Fig. 1) are vacuum chambers with a scintillating screen inside that can be moved into the beam by manipulators with stepper motors. The screens are usually invasive, *i.e.* the beam is absorbed or partially absorbed and deteriorated for downstream usage. The other imager components are outside of the vacuum chamber: optics, camera and optional optical neutral density filters; see Fig. 2 for a schematic design. The imagers differ for their field of view, spatial resolution, sensitivity and X-ray absorption of the scintillating screen. Details of the design are described by Koch *et al.* (2015). Fig. 1 shows two imagers in the SASE1 XTD2 photon tunnel as examples (SASE = self-amplified spontaneous emission, SASE1 = first branch of FEL radiation,

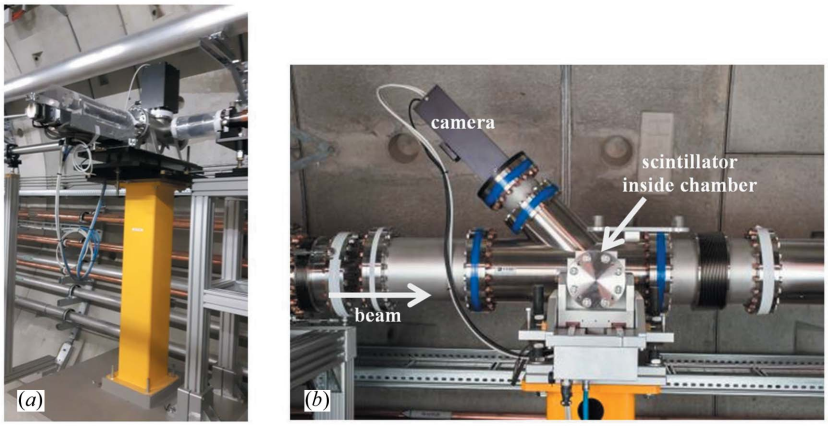

Figure 1
Diagnostic imagers in the SASE1 beamline tunnel XTD2. (*a*) FEL imager with a high spatial resolution of 10 µm. (*b*) Pop-In type II-45 imager with a wide field of view of 150 mm × 23 mm.

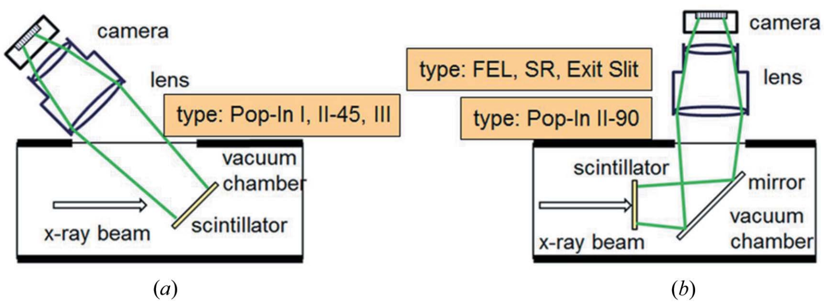

Figure 2
Photon diagnostic imagers: schematic optical design. (*a*) One type of device uses a scintillating screen under 45° with respect to the beam direction, (*b*) the other type images via a mirror with a screen under 90°.

XTD2 = X-ray distribution tunnel section 2). Table 1 in Appendix *A* summarizes the technical specifications of the installed imagers.

Apart from the standard tasks of imagers to provide beam position and shape (Grünert *et al.*, 2019; Koch *et al.*, 2015) there are some more particular applications. Each of these requires specific features as follows.

(1) Position correlation: using the intrinsic stable and well defined position calibration to check other components like the X-ray gas monitor (XGM).

(2) Feedback device: monitoring beam position with an almost transparent screen. During an experiment the screen can be left in the beam. The position information is used as feedback for beam steering with a mirror.

(3) Pulse-energy monitoring: using the high dynamic range of the FEL imager to monitor the absolute pulse energy but with lower accuracy than the XGM.

(4) Undulator tuning: measuring the *K* value of undulators with the highly sensitive Spontaneous Radiation imager in combination with a double-crystal monochromator (K-mono).

(5) Spectral imaging: together with a grating monochromator the Exit Slit imager records X-ray beam spectra without scanning.

(6) Single-pulse gating: imagers combined with fast multi-channel plate (MCP)-based shutters allow for recording of single pulses from the 4.5 MHz pulse trains.

(7) Gain curve measurement: relative pulse-energy monitoring with a variable number of active undulator segments to increase the laser intensity by optimizing the electron-beam orbit in the undulators.

Two issues in operating the imagers will be addressed: (i) radiation damage and (ii) spurious optical reflections.

2. Applications for diagnostic imagers

2.1. Position correlation

All imagers at the European XFEL have a fixed optical magnification, except for the Exit Slit imagers. As a result of the pixelated sensor, position information of the imagers is inherently stable and well calibrated by design. This makes the imagers complementary to correlate position information, *e.g.* to gas-based detectors. Fig. 3 shows the result for the XGM versus an imager (Pop-In type I) in the European XFEL SASE2 beamline tunnel XTD6. The specifications of the imager are given in Table 1. More details on position calibration of the XGM are given by Maltezopoulos *et al.* (2019) and by Sorokin *et al.* (2019). The position information of the XGM depends on the measurement of ion currents and is linear only over a restricted range of beam positions (Tiedtke *et al.*, 2008). For the imager, the position information was calculated by the centre of mass of a beam of ~0.6 mm in diameter and a pixel size of the imager of 9.1 µm.

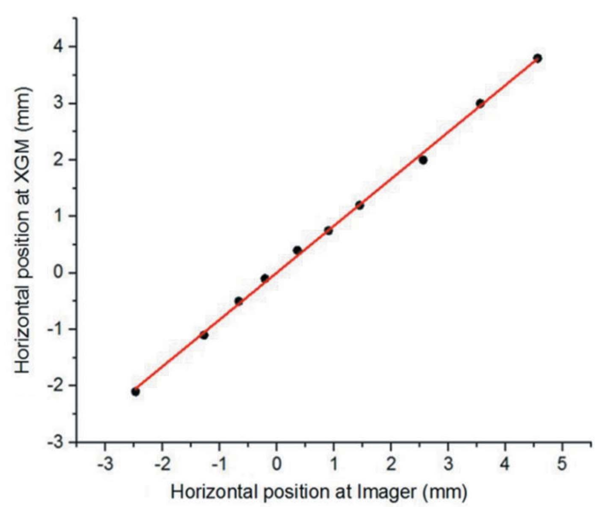

Figure 3
Position-correlation test between XGM and Pop-In imager in SASE2, XTD6 at 9.3 keV.

2.2. Feedback device for beam control

The beam position at the end of the beam-transport path at the instruments may drift or change for several reasons, *e.g.* a modified electron orbit in the undulators or alignment changes of components in the photon tunnels. Thin low-absorbing diamond screens are used to control the beam position in real time. A 50 µm thin diamond screen doped with boron of 40 mm × 40 mm had been installed, which has a low absorption of 5% at 9 keV.

Boron doping increases the fluorescence efficiency compared with undoped diamond by approximately a factor of 10^2 to 5% internal energy conversion efficiency (samples from Diamond Materials, Freiburg, Germany). The spectral emission is well adapted to the optical system; see Appendix *A*, Fig. 10. Other scintillators used in the diagnostic imagers are also shown. Boron nitride (BN) is another potential screen material for this feedback application as a result of its low X-ray absorption. This screen material is also installed in the FEL imager. The scintillator efficiencies are summarized in Table 2 in Appendix *A*.

2.3. Pulse-energy monitoring

The XGMs at the European XFEL are absolutely calibrated for pulse-energy measurements (uncertainty <10%; Tiedtke *et al.*, 2008). The FEL imager has been calibrated with respect to the XGM for low-accuracy pulse-energy measurements, either as a back-up device in case of XGM failures or for pulse-energy monitoring at tunnel positions where no XGM is available. The FEL imager does not measure the pulse-resolved energy and needs to be corrected for several parameters: image background, lens iris, neutral density filters, X-ray absorption and higher harmonics. The accuracy is estimated to be within a factor of two of the actual value. The sensitivity of the imagers achieves 20 µJ per pulse.

2.4. Undulator tuning

The individual segments of the long segmented undulator magnets need to be adjusted to the same *K* parameter, which is a quality parameter for efficient X-ray laser generation by the electron beam. From the spectral and spatial distribution of the spontaneous radiation this *K* parameter can be determined. The K-mono and the Spontaneous Radiation imager are available for these measurements; see Fig. 4 for a typical measurement (Freund *et al.*, 2019) from analysing single undulators segments, up to 400 m upstream. The Spontaneous Radiation imager has a high aperture optics and an efficient screen of GOS:Pr (Gd_2O_2S:Pr, Table 1) which provides a noise-equivalent photon energy of approximately 3 keV, *i.e.* a 3 keV photon generates a signal in this integrating sensor of the same level as the root-mean-square noise. The other diagnostic imagers are typically a factor of 10^2–10^3 less sensitive.

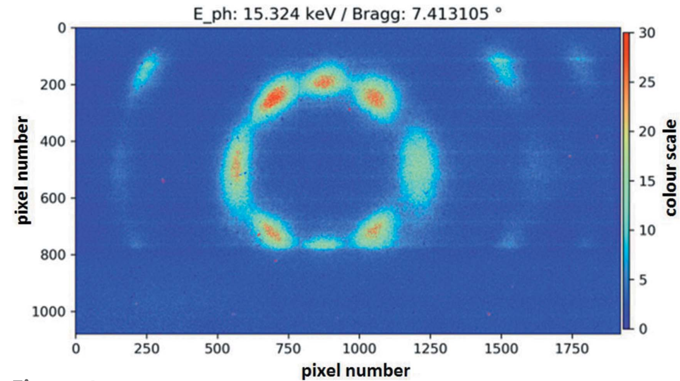

Figure 4
Spontaneous radiation from a single undulator segment (cell 23) at 900 eV. Image of the 17th harmonic (15.3 keV) using the K-monochromator with the Spontaneous Radiation imager in the SASE3 beamline tunnel XTD10.

2.5. Spectral analysis of a photon beam in SASE3

A cylindrically shaped focusing mirror and a grating monochromator (La Civita *et al.*, 2014) in SASE3, XTD10, provide spectral information about the FEL beam in the plane of the Exit Slit imager. The characteristics of the Exit Slit imager are given in Table 1. First commissioning shows images of the first and second order of the grating at 852 eV; see Fig. 5. The calibration is done by using Ne gas in an upstream gas attenuator chamber.

The imager has two optical systems that can be swapped. The first provides a wide field of view at high spatial and spectral resolution, and the second provides single-pulse gating (for the 4.5 MHz pulse train) with an MCP as a fast optical shutter (Table 1). The commissioning of the MCP-based system is ongoing.

2.6. Single-pulse gating

The Exit Slit imager provides an optical system with a fast shutter (MCP) to separate a single pulse out of a 4.5 MHz pulse train (see also Section 2.5). The time response to a single pulse per train is characterized (Fig. 6). At 4.5 MHz, successive pulses are separated by 220 ns. From Fig. 6(*a*) the signal level after 220 ns is 10%. The remaining signal beyond 220 ns would add to the next pulse (crosstalk). In general, the time-response functions of several successive pulses have to be convolved to obtain the system response.. The parameters determining the time response to X-ray pulses are the response of both the scintillator and the MCP. Optical radiation of the accelerator is used to measure the time response of the MCP only, without the influence of the scintillator; see the red curve in Fig. 6(*b*). The curve shows that the MCP response is faster than the X-ray response, *i.e.* the scintillator properties determine the time decay.

The single-pulse gating is interesting in different respects. For example, the spectral characteristics of each pulse may vary within a pulse train; additionally, SASE1 operation may influence pulses in SASE3. Both effects can be studied in the future with single-pulse gated imagers.

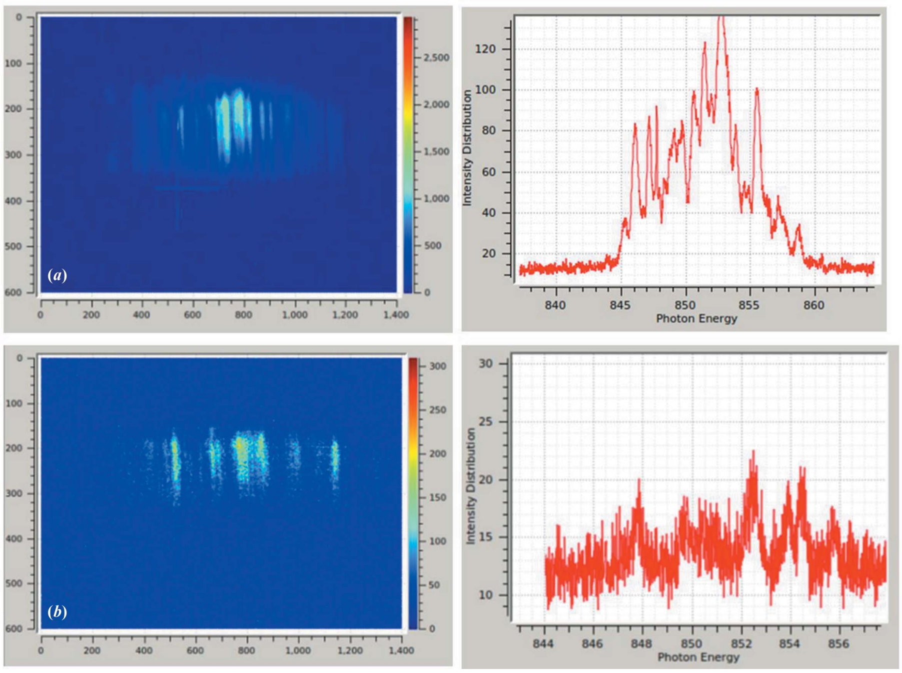

Figure 5
Spectrum of the XFEL beam, SASE3, SCS, 852 eV, single pulse per train (*a*) first order, (*b*) second order diffraction images and corresponding plots of signal versus photon energy.

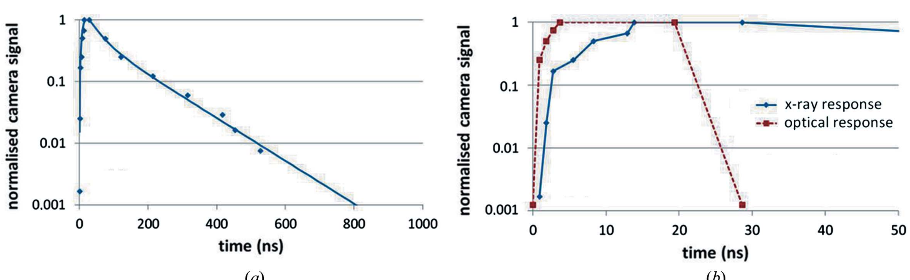

Figure 6
Time response of SASE3 Exit Slit imager with MCP gating at 900 eV. (*a*) The decay time is limited by the scintillator decay (blue solid line). (*b*) The response to optical radiation (red dashed line) shows the limits of the detection system. The MCP gate opening time was 19 ns.

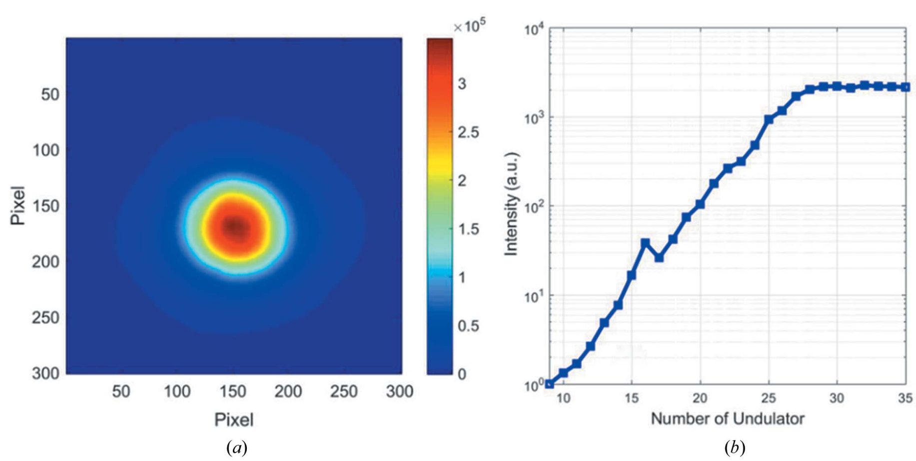

Figure 7
Photon gain curve measurements. The FEL imager is used to record the intensity for a variable number of active undulators. Beam conditions in SASE1: 8.3 keV, 1.2 mJ, including harmonics, 10 Hz, 1 pulse per train. (*a*) Image of beam, pixel size 9.1 µm; (*b*) gain curve.

2.7. Photon gain curve measurements

Imagers are useful tools for gain curve measurements where the electron orbit through the variable-gap undulators is optimized by tracing the photon pulse energy versus the number of active undulators with closed gap. Fig. 7 gives the results of a typical test. Amongst all the imagers, the FEL imager is particularly suited for such measurements thanks to its high dynamic range: the camera dynamic range combined with its electronic gain is 10^5; motorized neutral density filters add to this range a further 10^6, whereas the high-absorbing grey filters (ND2 = 10^{-2} and ND3 = 10^{-3}) are seldom used. The noise-equivalent pulse energy is approximately 20 µJ, depending on photon energy and beam size.

3. Issues and solutions

3.1. Radiation damage

Radiation damage is distinguished in dose-related effects and single-shot or multiple-shot damage. Dose-related effects depend on the specific material, *e.g.* changes in electronic bonds or creation of colour centres. Single-shot or multiple-shot damage is estimated by the threshold of local melting of the material (Koch *et al.*, 2015).

In the past months, both effects have been observed. YAG screens have been damaged locally by a focused beam at 900 eV, single pulse per train: either its surface was damaged or holes were created; no screen broke apart. The threshold was measured to be approximately a factor of four higher than the theoretical melting threshold suggested by Koch *et al.* (2015). The measured threshold in the case of the YAG screens is ~1 mJ per 0.05 mm^2, at 900 eV, single pulse per train, 10 Hz. The deviations with respect to the model are under investigation. Measurements of single-shot damage at 269 eV show a similar threshold for YAG, within a factor of two (Burian *et al.*, 2015). Fig. 8 shows a damaged screen.

Dose effects have been observed for BN for an accumulated dose of 10 kGy. The material becomes slightly brownish

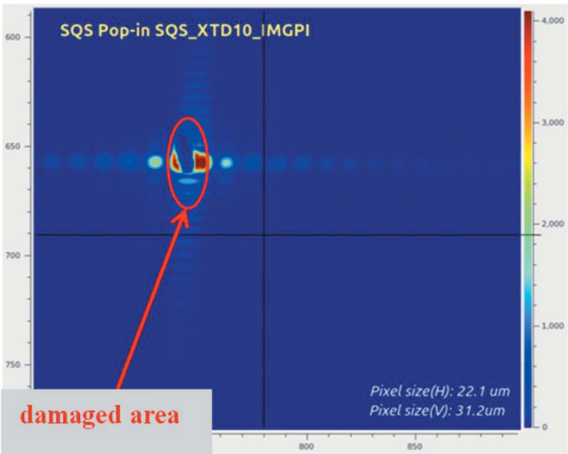

Figure 8
Single-shot damage of a YAG:Ce screen. A hole of 0.2 mm × 0.5 mm is observed in the 50 µm-thick screen which corresponds to the focused beam size.

with a reduced light output by a factor of less than two; the effect disappears after some days.

3.2. Spurious reflections by optical radiation

Spurious reflections within the optical system have been observed for the diagnostic imagers with mirrors under 90° with respect to the X-ray beam axis and transparent scintillating screens [Fig. 2(*b*)]; see Fig. 9(*a*). The root cause is optical radiation within the beam pipe, probably from dipole magnets in the electron beamline. This radiation projects an image of the iris of the lens onto the camera via reflections within the optical system, including reflections from the scintillator. The surface roughness of the BN scintillator suppresses these reflections to a large extent. For the other imagers with scintillators under 45° these reflections do not occur since the visible light, parallel to the X-ray beam, does not enter the optical system. The origin of the optical radiation and a quantitative understanding are under study.

The optical radiation can be suppressed by an aluminium coating (50 nm thick) on the YAG screen; Fig. 9(*b*). The Al coating has low X-ray absorption (<10% down to 200 eV) and rejects the visible light within the wavelength range of the camera's sensitivity.

4. Summary and outlook

Photon diagnostic imagers for the XFEL beam employing scintillator screens proved to be useful for a variety of beam characterization beyond their primary use for determination of beam position and shape. Improvements concerning spurious reflections are planned. The radiation-damage issue will be addressed by real-time control ('watch dog') of critical parameter thresholds.

Single-pulse gating and recording of multiple pulses within 4.5 MHz pulse trains with single-pulse resolution for diagnostic purposes remains challenging. MCP gating with 20 ns time response and repetition rates of tens of kHz can record multiple pulses within the 600 µs-long XFEL pulse train. Successive pulses with a time separation of 220 ns can also be recorded with optical high-speed cameras. For both future options, the YAG:Ce scintillator is close to its limit; therefore, other scintillators will be investigated. The MCP-gating is designed in a modular way, with separate components of lenses, MCP and camera. The intention is to test this design for future retrofit developments of other imagers.

APPENDIX *A*
Imager and scintillator specifications

Table 1 gives specifications of the installed photon diagnostic imagers. Table 2 gives the efficiencies of the scintillators installed in the diagnostic imagers. Fig. 10 shows the spectral

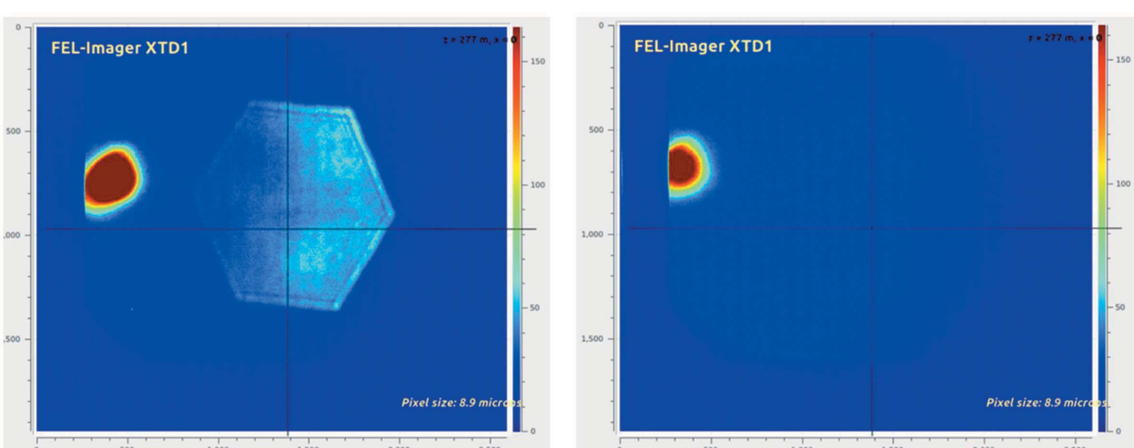

(*a*) (*b*)

Figure 9
Spurious reflections of optical light within the optical system of the X-ray imagers. (*a*) A hexagon-shaped reflection from the iris of the lens is visible when using a YAG screen. (*b*) The reflection effect disappears changing to an Al-coated YAG screen. Screens can be exchanged within seconds. The images were recorded during beam alignment; the FEL beam is on the left side of each image.

Table 1
Specifications of the installed photon diagnostic imagers: 8 different designs, 24 devices.

All imagers operate at 10 Hz and average over a pulse train of 600 µs; only the Exit Slit imager allows single-pulse gating. The scintillators that are mounted under 45° have a rectangular pixel size. For more details, see Grünert *et al.* (2019). GOS = Gd_2O_2S, YAG = $Y_3Al_5O_{12}$.

Imagers	Basic applications	Field of view (mm)	Resolution (µm) (FWHM)	Scintillators	Remarks
Transmissive (OTRC)	Beam position, close to undulator pointing with FEL-imager → low-invasive for high-energy beam	25 × 25	25	YAG:Ce, diamond:B	Highest beam intensity at this imager (2× FEL)
Spontaneous Radiation imager	Spontaneous radiation with K-mono undulator characterization → highest sensitivity	27 × 15	30	YAG:Ce, GOS:Pr	High sensitivity: noise-equivalent photon energy ≃ 3 keV r.m.s.
FEL imager	Beam position, profile pointing with Transmissive imager → high single-shot resistant with diamond and BN → high spatial resolution	22 × 16	10	YAG:Ce, diamond:B BN	diamond damage: >7 pulses per train at 260 eV, 10 mJ, >140 pulses per train at 3 keV, 3.7 mJ
Pop-In type I	Mirror and monochromator alignment	40 × 40	50	YAG:Ce	Scintillator under 45° resolution distortion
Pop-In type II-45	Mirror and monochromator alignment	150 × 40	120	YAG:Ce	Scintillator under 45° resolution distortion
Pop-In type II-90	Mirror and monochromator alignment	100 × 120	130	YAG:Ce	
Pop-In type III	Mirror and monochromator alignment	200 × 40	80	YAG:Ce	Scintillator under 45° resolution distortion
Exit-Slit imager (1)	Spectral resolution measurement optics for high resolution	40 × 40	14	YAG:Ce	Zoom 22 mm × 16 mm possible
Exit-Slit imager (2)	Spectral resolution measurement single-pulse gating with MCP	31 × 17	23	YAG:Ce	Zoom 8.2 mm × 4.6 mm possible

Table 2
Efficiencies of the scintillators installed in the diagnostic imagers.

The absolute conversion efficiency of YAG:Ce is used as a reference value (Crytur, Turnov, Czech Republic). The screens are 40–100 µm thick. Corrected for spectral sensitivity of detector and X-ray absorption. Components: X-ray source with copper anode (PANalytical), optical lens (Kowa LM 25SC) and CCD camera (Basler avA1900-50gm). GOS = Gd_2O_2S, YAG = $Y_3Al_5O_{12}$.

Scintillating screen	YAG:Ce	Diamond:B	BN	GOS:Pr
Internal energy conversion efficiency (generated radiation/absorbed radiation)	0.080	0.052	0.0033	0.15
Screen emission efficiency (perpendicular to screen, relative to YAG)	1.0	0.38	0.27	13
Morphology	Transparent screen	Transparent screen, CVD	Scattering screen, pyrolytic hexagonal ceramics, CVD	Scattering screen, ceramics
Manufacturer	Crytur, Czech Republic	Diamond Materials, Germany	CVT, Germany	Laboratory sample

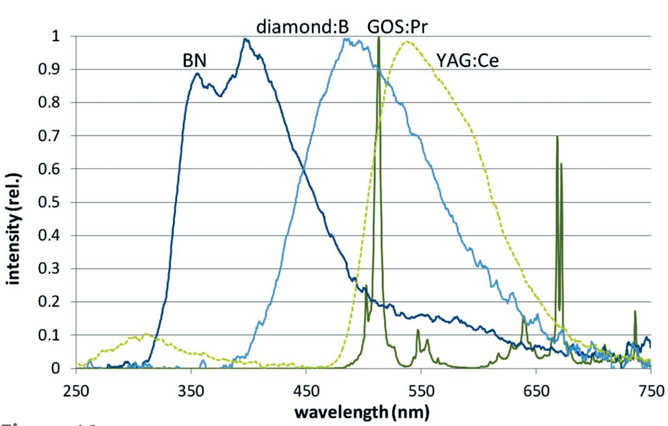

Figure 10
Spectral emission of the scintillating screens under X-ray excitation used in the diagnostic imagers. An X-ray generator with copper anode (PANalytical) and a grating spectrometer with a CCD line sensor (Laser 2000, RPS-Mini-Wide UV) were used, characteristic radiation at 8 keV, GOS = Gd_2O_2S, YAG = $Y_3Al_5O_{12}$.

emission of the scintillating screens under X-ray excitation used in the diagnostic imagers.

Acknowledgements

We would like to thank many colleagues from the European XFEL Optics group, especially the Commissioning team for their help and feedback. This feedback was essential in finding shortcomings and eventually improving the imagers in daily operation. Special thanks to L. Samoylova for providing an image on the spurious reflections, D. La Civita and N. Gerasimova for images and software for the SASE3 spectrometer, J. Liu for a photon gain curve plot and T. Mazza for the image of the damaged screen. We are also grateful to the European XFEL science-support groups CAS, AE, and ITDM who were essential for the operation, control and bug-fixing of the imager systems.

References

Burian, T., Hájková, V., Chalupský, J., Vyšín, L., Boháček, P., Přeček, M., Wild, J., Özkan, C., Coppola, N., Farahani, S. D., Schulz, J., Sinn, H., Tschentscher, T., Gaudin, J., Bajt, S., Tiedtke, K., Toleikis, S., Chapman, H. N., Loch, R. A., Jurek, M., Sobierajski, R., Krzywinski, J., Moeller, S., Harmand, M., Galasso, G., Nagasono, M., Saskl, K., Sovák, P. & Juha, L. (2015). *Opt. Mater. Express*, **5**, 254–264.

Freund, W., Fröhlich, L., Karabekyan, S., Koch, A., Liu, J., Nölle, D., Wilgen, J. & Grünert, J. (2019). *J. Synchrotron Rad.* **26**, 1037–1044.

Grünert, J., Planas, M., Dietrich, F., Falk, T., Freund, W., Koch, A., Kujala, N., Laksman, J., Liu, J., Maltezopoulos, Th., Tiedtke, K., Jastrow, U. F., Sorokin, A. A., Syresin, E., Grebentsov, A. & Brovko, O. (2019). *J. Synchrotron Rad.* **26**, 1422–1431.

Koch, A., Freund, W., Grünert, J., Planas, M., Roth, T., Samoylova, L. & Lyamayev, V. (2015). *Proc. SPIE*, **9512**, 95121Q.

La Civita, D., Gerasimova, N., Sinn, H. & Vannoni, M. (2014). *Proc. SPIE*, **9210**, 921002.

Maltezopoulos, T., Dietrich, F., Freund, W., Jastrow, U. F., Koch, A., Laksman, J., Liu, J., Planas, M., Sorokin, A. A., Tiedtke, K. & Grünert, J. (2019). *J. Synchrotron Rad.* **26**, 1045–1051.

Sorokin, A. A., Bican, Y., Bonfigt, S., Brachmanski, M., Braune, M., Jastrow, U. F., Gottwald, A., Kaser, H., Richter, M. & Tiedtke, K. (2019). *J. Synchrotron Rad.* **26**, 1092–1100.

Tiedtke, K., Feldhaus, J., Hahn, U., Jastrow, U., Nunez, T., Tschentscher, T., Bobashev, S. V., Sorokin, A. A., Hastings, J. B., Möller, S., Cibik, L., Gottwald, A., Hoehl, A., Kroth, U., Krumrey, M., Schöppe, H., Ulm, G. & Richter, M. (2008). *J. Appl. Phys.* **103**, 094511.

Tschentscher, T., Bressler, C., Grünert, J., Madsen, A., Mancuso, A. P., Meyer, M., Scherz, A., Sinn, H. & Zastrau, U. (2017). *Appl. Sci.* **7**, 592.